Journal of Catalysis 266 (2009) 98–105

Contents lists available at ScienceDirect

Journal of Catalysis

journal homepage: www.elsevier.com/locate/jcat

CO oxidation on $Au/FePO_4$ catalyst: Reaction pathways and nature of Au sites

Meijun Li, Zili Wu, Zhen Ma, Viviane Schwartz, David R. Mullins, Sheng Dai, Steven H. Overbury *

Chemical Sciences Division, Oak Ridge National Laboratory, Oak Ridge, TN 37831, United States

ARTICLE INFO

Article history:
Received 25 March 2009
Revised 25 May 2009
Accepted 27 May 2009
Available online 25 June 2009

Keywords:
Au catalyst
$FePO_4$
Iron phosphate
CO adsorption
Catalytic CO oxidation
Redox
FTIR
Raman spectroscopy
XANES
Mechanism

ABSTRACT

In situ FTIR spectroscopy coupled with downstream mass spectrometry has been used to clarify the pathways for room temperature (rt) CO oxidation over iron phosphate-supported Au catalyst. The charge state of Au on $Au/FePO_4$ after calcination, reduction, or under reaction conditions was assessed by both FTIR spectroscopy (CO probing) and X-ray absorption near edge spectroscopy (XANES). Results from both approaches show that cationic gold species dominate the surface after pretreatment in O_2 at 200 °C. A portion of the cationic gold on $Au/FePO_4$ can be reduced by the initial CO adsorption at rt, and subsequently repeated CO exposures do not reduce the remaining cationic Au. FTIR and Raman results from cycled CO reduction and O_2 reoxidation of $Au/FePO_4$ indicate that there are active structural oxygen species on the surface of $Au/FePO_4$ that can be consumed by CO and then replenished by gaseous O_2 at rt. Au activates both CO and O_2 so that the $FePO_4$ support can undergo reduction (by CO) and reoxidation (by O_2) cycles. The results of CO oxidation with labeled $^{18}O_2$ suggest the operation of two parallel reaction pathways at rt: (1) a redox pathway in which $FePO_4$ supplies active oxygen and (2) a direct pathway on metallic Au, *via* either Langmuir–Hinshelwood or Eley–Rideal mechanism, in which gas phase O_2 provides the active oxygen.

1. Introduction

It is well established that when properly prepared and supported, Au can be highly effective for the oxidation of CO at very low temperatures [1–3]. Among the conclusions that may be extracted from the body of work devoted to the catalytic properties of supported gold catalysts are (1) the importance of the gold oxidation state in determining the active site and (2) the key role that the support plays in creating an active and stable catalyst [4]. Contradictory hypotheses have been advanced to describe the active sites, and the nature of the reactive oxygen intermediates remains elusive. There are many observations indicating that metallic gold atoms or small metallic gold particles are the active sites in the CO oxidation reaction [5–9]. However, some authors have proposed that cationic gold species, stabilized by an interaction with the support, are more active than Au^0 [10–16]. The apparent discrepancy may result from the dependence upon the support type, the catalyst preparation method, or upon whether the activity is measured for CO oxidation or water–gas shift, the two most common reactions used for performance testing. The morphology of the Au particles, possibly determined by the support, also appears to play an important role [17–20].

Many high surface area oxides have been tried as supports for Au. Metal oxides used as Au supports may be classified as inert or active according to their reducibility [21,22]. Thus, Al_2O_3, SiO_2, and MgO are included within the inert supports, while reducible transition metal oxides such as Fe_2O_3, MnO_2, TiO_2, and CeO_2 may be considered as active supports. The catalytic activity of the latter group may be hypothesized to depend upon the ability of the support to provide reactive oxygen to the catalytic system. However, the relationship between activity and oxide reducibility is not straightforward. Support reducibility does not guarantee high activity, and if properly prepared and pretreated, Au can be very active on non-reducible supports such as SiO_2 [23,24]. Several mechanisms have been proposed to explain the enhanced activity at the metal–oxide interface including the presence of highly reactive surface gold atoms at growth steps [25], the ease of charge transfer at the interface [26], and in the case of reducible supports, the ability to provide activated oxygen that can be trapped at the reaction sites [22]. Whatever be the mechanism, it is evident that the interaction between the support and gold must be tailored for performance enhancement.

Although there are numerous reports on oxide-supported Au catalysts, there are fewer investigations of Au supported on salts or complex oxides. Recently, several researchers have used metal carbonates [27], hydroxyapatite ($Ca_{10}(PO_4)_6(OH)_2$) [28–30], and orthovanadates ($LaVO_4$) [31] as support materials for preparing Au catalysts. An $Au/BaCO_3$ catalyst was found to be active for CO oxidation at 25 °C, but it deactivates quickly on stream [27]. $Au/Ca_{10}(PO_4)_6(OH)_2$ catalysts were reported to have activity in water–gas shift and CO oxidation above 100 °C and 50 °C,

* Corresponding author. Fax: +1 (865) 576 5235.
E-mail address: overburysh@ornl.gov (S.H. Overbury).

0021-9517/$ - see front matter © 2009 Elsevier Inc. All rights reserved.
doi:10.1016/j.jcat.2009.05.019

respectively [28,29,32,33]. Recently, metal phosphates ($LaPO_4$, $FePO_4$, $AlPO_4$, etc.) have been explored as supports for Au catalysts [34,35]. Gold nanoparticles can be well dispersed on some metal phosphate supports, and show significant activity at room temperature (rt). Since some metal phosphates are useful in acid catalysis and selective oxidation [36–38], Au/metal phosphates may also be useful for many other reactions. The application of the phosphate-based supports opens up a new avenue in the search for highly active, stable, and selective gold catalysts for a number of catalytic reactions. In addition, studies of this type of supports may shed new light on the reaction mechanism associated with gold-based catalysts. In this work, we present the first observation that the presence of Au species assists the storage of active oxygen species in $FePO_4$, which opens up two channels for CO oxidation on Au/$FePO_4$ at rt: Mars–van Krevelen (redox) and direct (e.g. Langmuir–Hinshelwood) mechanisms.

2. Experimental

2.1. Preparation of Au/$FePO_4$

The $FePO_4$ support (surface area 28 m^2/g) was purchased from Aldrich. Au was deposited onto $FePO_4$ using deposition–precipitation (DP) with $HAuCl_4$ precursor. Briefly, 0.6 g $HAuCl_4$ was dissolved in 100 ml deionized (DI) H_2O, the pH of the solution was adjusted to 10 with 1 M KOH solution and 2.0 g $FePO_4$ was added. The pH value of the solution dropped after adding $FePO_4$, and was re-adjusted to approximately 10 with KOH solution. The suspension was stirred at 80 °C for 2 h, and was then filtered and washed with DI H_2O. The product was dried at 40 °C for two days and stored without further calcination in this "as-synthesized" state until used in the following experiments. Au loading was 5.5 wt% as determined by ICP analysis on an IRIS Intrepid II XSP spectrometer (Thermo Electron Corporation). The catalyst used here is the same as that used previously in a survey of phosphate-supported Au catalysts [35]. In that work the catalysts were characterized by XRD, TEM, and SEM, and following treatments at 200 °C in O_2, conditions that mimic those used herein and so this reference provides additional information about the catalyst used in the current work. Additional microscopy was performed in the current work following oxidative treatments.

X-ray fluorescence confirmed the Au loading but indicated a high level of K (9 wt%). K on the catalyst is attributed to ion exchange of H terminating the surface phosphate groups during the Au DP synthesis. A repeat of the synthesis, taking extra care to wash well after DP to remove K^+ and Cl^-, did not eliminate the K from the final dried sample. It was hypothesized that the K^+ terminates surface phosphate groups, and therefore could be replaced with H^+ by ion exchange with acid. However, attempts to exchange with HCl led to dissolution of the support. Exchange with acetic acid did decrease K loading somewhat but deactivated the catalyst, similarly to previously reported effect of acid [32]. Therefore all experiments were conducted on the K-containing catalyst. It should be noted that ammonium hydroxide must not be used as an alternative to KOH because a potentially explosive mixture may be formed [3].

2.2. Transient FTIR experiments

The chemisorption and reaction experiments were performed using a transient gas switching system for probing catalytic pathways. FTIR spectroscopy was conducted in a diffuse reflectance cell (cell volume about 6 cm^3) in a Nicolet Nexus 670 FTIR spectrometer using a MCT/A detector with a spectral resolution of 4 cm^{-1}. After the desired pretreatments, a background spectrum was collected from the sample using 256 scans and 4 cm^{-1} resolution. Diffuse reflectance FTIR (DRIFTS) spectra were obtained by subtracting the background spectrum from subsequent spectra, and such difference spectra are reported herein. Gases leaving the DRIFTS cell were analyzed using a downstream gas sampling quadrupole mass spectrometer (QMS, Pfeiffer–Balzer Omnistar) equipped with a 1-m long gas sampling capillary followed by an apertured entrance into the turbo-pumped QMS chamber.

Prior to data collection, as-synthesized Au/$FePO_4$ was pretreated at 200 °C in a flowing gas stream of either 2%O_2/He (O_2-pretreated sample) or 4%H_2/He (H_2-pretreated sample), and then cooled to rt in He. Then a selected gas stream was introduced onto the sample at a total flow rate of 15 cm^3/min. The gas stream was either pure He, CO (2%CO/2%Ar/He), or a reaction mixture of CO and O_2 at a ratio of 1:4 (2%CO/2%Ar/He mixed with 2%O_2/He). In a typical switching experiment, two gas streams, flowing either through the DRIFTS cell or to a vent, were abruptly interchanged using a four-way switching valve located upstream from the cell. The times described in the manuscript are relative to the time ($t = 0$) at which the inlet valve was switched. At the flow rate used, a delay time of about 20 s is required to reach the IR cell and about 40 s to reach the QMS. Alternatively, in a typical pulsing experiment, a six-way valve could be used to introduce a 0.5-ml gas pulse into one of the gas streams. Both pulsing and switching experiments were carried out.

2.3. X-ray absorption near edge spectroscopy (XANES) measurements

XANES data at the Au L_{III}-edge were collected at beam line X18b at the NSLS, Brookhaven National Laboratory. XANES was performed in transmission mode using two ion chambers placed in the beam path. Absorption measurements were made in a quartz tube (50 cm long × 2.4 cm diameter) which could be heated for sample treatments or for *in situ* measurements. For each run, a weighed amount of fresh catalyst (about 100 mg) was mixed with 100 mg of BN and loosely pressed into a 12-mm-diameter pellet. BN was added to provide structural integrity to the wafer without interfering with X-ray absorption. XANES experiments were performed under reduction, calcination, or reaction conditions.

2.4. UV Raman spectroscopy

Raman spectra of differently treated Au/$FePO_4$ were collected at rt using an *in situ* Raman reactor (Linkam CCR1000) on a triple-stage spectrometer (PI Acton Trivista 555) with laser excitation at 325 nm (HeCd laser, Melles–Griot). The spectral collection time was typically 5 min with laser power of 4 mW at the sample position. Cyclohexane was used as a standard to calibrate the Raman shifts. *In situ* Raman spectra of Au/$FePO_4$ were obtained following exposure to 1%CO/He, 16% O_2/He, or a mixture of 1%CO–5%O_2 in He after pretreating either in 16% O_2/He at 200 °C or in 4% H_2/Ar at 200 °C.

3. Results

3.1. CO adsorption on Au/$FePO_4$ with different treatments

First, CO adsorption was investigated on an O_2-pretreated sample by a switching experiment. A gas switch from He to a CO–He mixture was conducted at rt and monitored by FTIR and QMS, and the results are shown in Fig. 1A and the inset. A band at 2169 cm^{-1} due to adsorbed CO appears immediately after switching. Two other bands at 2129 and 2114 cm^{-1} develop and dominate the spectra as more CO adsorbs on the surface. These CO bands saturate after about 20 min and show no further change. In contrast, $FePO_4$ (i.e. Au-free) pretreated in a similar way exhibited no CO adsorption under the same conditions (not shown). We

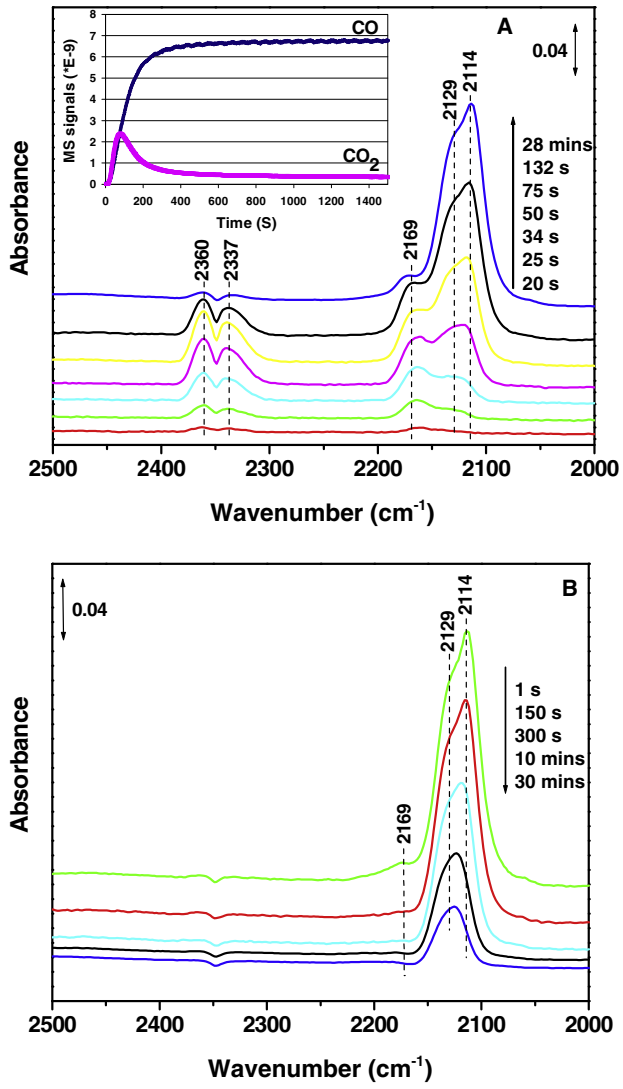

Fig. 1. IR spectra and QMS (inset) results for CO adsorption at rt on O_2-pretreated $Au/FePO_4$: (A) as a function of adsorption time after switching from He to CO and (B) during desorption at rt after the CO flow is switched to He.

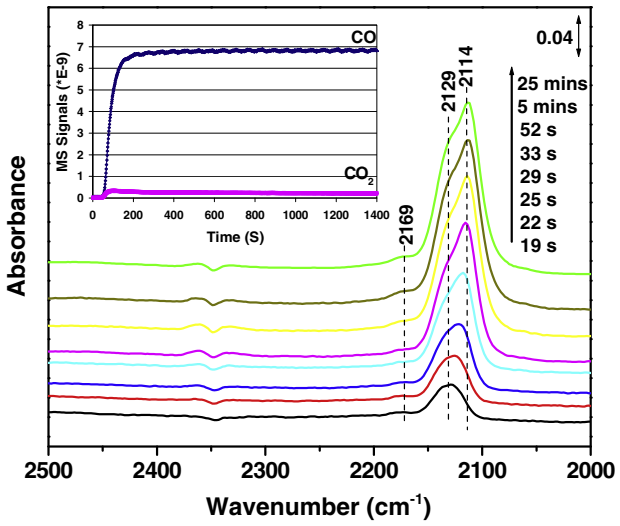

Fig. 2. IR spectra and QMS (inset) results for CO re-adsorption at rt onto O_2-pretreated $Au/FePO_4$ after flushing away most of the adsorbed CO by He.

could find no literature describing the assignments of CO adsorption on $FePO_4$ or on phosphate-supported Au. According to IR studies of CO adsorption on Au/Fe_2O_3 [39,40] and on other supported Au catalysts [41], the bands at 2169 and 2129 cm^{-1} may be assigned to CO adsorbed on cationic or partially charged Au ($Au^{\delta+}$, $0 < \delta \leqslant 1$) with two different charges. The band at around 2114 cm^{-1} is due to CO adsorbed on metallic Au (Au^0). Upon switching the gas back to He, the desorption of CO was observed as shown in Fig. 1B. The bands at 2129 and 2114 cm^{-1} still dominate after most of the surface CO has desorbed. Subsequent re-adsorption of CO yielded results that were different from those shown in Fig. 1A, namely the bands at 2114 and 2129 cm^{-1} dominate the spectra from the very beginning with only a weak shoulder at 2169 cm^{-1} as shown in Fig. 2. Repeated CO desorption/adsorption cycles led to the growth of IR features during adsorption, which was similar to that shown for the second adsorption process in Fig. 2.

The variation in the CO band during the first CO adsorption (initial growth of the peak at 2169 cm^{-1} followed by the growth of the 2129 and 2114 cm^{-1} peaks) is likely not due to a change in particle size distribution since TEM results show essentially the same mean particle size and standard deviation for the O_2-treated $Au/FePO_4$ sample (3.5 ± 0.6 nm) as for the sample after repeated CO exposures and heat treatments at 200 °C (3.9 ± 0.8 nm). These agree well with previous Au particle sizes for $Au/FePO_4$ described as being 1-3 nm [35]. Nor is the variation due to a coverage-induced shift in the stretching frequency, since Fig. 1B shows that the peak at 2169 cm^{-1} does not reappear upon decreasing coverage during desorption. Instead, this irreversible change is related to a change of Au oxidation state during the CO adsorption. Apparently, reduction of a portion of the cationic Au species (2169 cm^{-1}) occurs during CO adsorption at rt on the O_2-pretreated $Au/FePO_4$ catalyst. In experiments using pulses of CO on a fresh O_2-pretreated sample, only the peaks at 2169 and 2129 cm^{-1} appear during the first pulse, confirming that only the cationic Au adsorbs CO on the initially oxidized surface and that the reduced Au that subsequently appears must result from reduction of this cationic Au.

Room temperature reduction, indicated by the CO adsorption experiments, is verified by the simultaneous evolution of CO_2 during the initial stage of the first CO adsorption (inset of Fig. 1A). It is also supported by XANES measurements shown in Fig. 3. In Au L_{III} XANES measurements, an absorption peak at 11,920 eV is indicative of oxidized Au [42], and therefore its decreasing intensity signals the reduction of Au. Our XANES measurements confirmed that

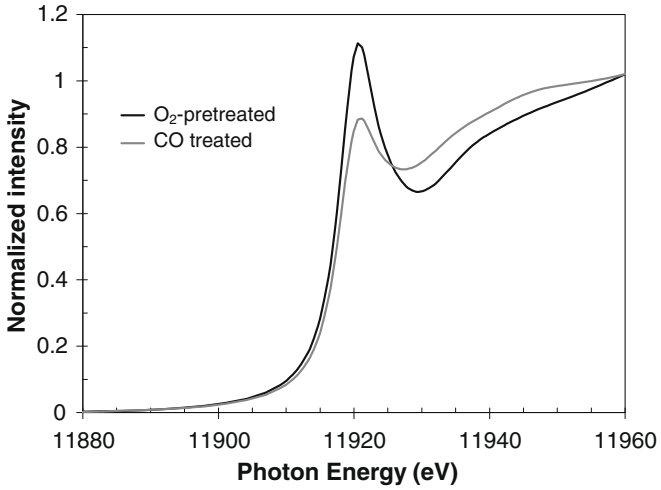

Fig. 3. XANES scans on 5.5 wt% $Au/FePO_4$: (a) after treating in 10% O_2 in He for 2 h at 200 °C and cooling down to rt in He and (b) then followed by about 20 min in 5% CO/ He at rt.

a portion of the cationic gold on the fresh sample is reduced by O_2-pretreatment at 200 °C but a peak due to cationic Au remains (Fig. 3a). Further reduction was observed after introduction of CO flow (Fig. 3b), indicating that an additional portion of the cationic Au may be reduced by rt exposure to CO. More extensive data were obtained for a similarly prepared sample with lower Au loading (2.6 wt% Au/$FePO_4$) that reproduced these trends (not shown). For the sample with lower Au loading, repeated scans during CO exposure confirmed initial partial reduction, but there was incomplete reduction of the cationic Au even after more than 1 h exposure to CO. Persistence of cationic Au is consistent with the observation of the IR bands at 2130 and 2169 cm^{-1} after repeated CO adsorptions on Au/$FePO_4$.

CO adsorption was also investigated on a H_2-pretreated sample. Pulsing CO at rt in He leads to the appearance of only one band at 2103 cm^{-1}, assignable to CO adsorption on metallic Au, as shown in Fig. 4. This peak is sharp and remains at 2103 cm^{-1} for the full range of coverages achieved during the pulse. There is no signature of higher frequency CO stretches indicative of cationic Au species, suggesting that the H_2-pretreatment reduces all Au. Interestingly, both IR and QMS results (inset of Fig. 4) show that a small amount of gas phase CO_2 is produced during the pulse. Since there is no O_2 in the gas flow, the only available oxygen source for this H_2-pretreated sample is the structural oxygen of $FePO_4$, which implies that $FePO_4$ is not completely reduced in H_2 at 200 °C. Nevertheless, the result shown in Fig. 4 implies that the formation of CO_2 during CO adsorption is not solely due to the reduction of cationic Au (e.g. Au oxide). Instead, part of the CO_2 evolved during rt chemisorption must have come from the reduction of $FePO_4$ by CO in both cases.

It is an unexpected result that rt CO can remove some of the oxygen after a 200 °C reduction in H_2. To test that the observed CO_2 evolution was not due to some spurious effect of the method, similar CO pulses were performed in a blank experiment on an Au-free $FePO_4$ sample, and no CO_2 production was observed in that case. In another test, the Au/$FePO_4$ was reduced in CO at 200 °C, and in subsequent rt CO pulsing experiments no CO_2 production was observed. Evidently, CO is more effective than H_2 at reducing the phosphate in the Au catalysts.

3.2. CO_2 formation and rt redox property of $FePO_4$ in Au/$FePO_4$

To explore the nature of the active oxygen leading to CO_2 evolution further, repeated sets of CO adsorptions (by gas switching) were performed on the O_2-pretreated Au/$FePO_4$. After an initial rt CO adsorption and desorption, the sample was subjected to an intermediate O_2 flow at rt and then to He purging before performing another CO adsorption. In this second CO adsorption, which is shown in Fig. 5, the IR spectra are now dominated by 2114 and 2129 cm^{-1} bands from the beginning of the adsorption, as is the case with CO re-adsorption process shown in Fig. 2. In particular, the 2169 cm^{-1} peak corresponding to cationic Au is much decreased. However, CO_2 production is observed (inset, Fig. 5), indicating that there are active oxygen species on the surface of Au/$FePO_4$ that are not due to the oxygen associated with cationic Au. Repeating the sequence of CO adsorption followed by rt O_2 exposure multiple times on the same sample gave almost identical growth of CO bands (position and relative intensity), and CO_2 evolved during each CO adsorption cycle as is shown in the inset of Fig. 5. Therefore, it appears that the active oxygen species that is consumed to evolve CO_2 can be replenished by gas-phase O_2 at rt without variation in the relative amounts of Au species.

Replenishment of active oxygen is also possible on H_2-pretreated Au/$FePO_4$, which is devoid of any cationic Au. This was confirmed by a similar experiment of repeated CO pulses onto the H_2-pretreated sample immediately after an exposure to O_2 flow at rt and He purge. Fig. 6 shows that only the CO band at 2108 cm^{-1}, associated with Au^0, is present in the spectrum. A high ratio of CO_2 to CO was obtained during the CO pulse, as indicated both in the gas phase CO_2 IR bands and in the evolved gas measured by the QMS (inset Fig. 6). The CO_2 level is also high compared with the experiments shown in Fig. 4 where there was no prior O_2 exposure at rt. Repeating the sequence of CO pulses on the same sample gave almost identical growth of CO bands (position and relative intensity). The amount of CO_2 evolved during the second CO pulse was slightly decreased compared with that obtained during the first CO pulse as shown in the inset of Fig. 6 because of active oxygen consumption during the first pulse. This suggests that part of the oxygen species that may be removed by the H_2-pretreatment at 200 °C can be regenerated by gas-phase O_2 at rt.

The source of the active oxygen species could be chemisorbed oxygen from rt O_2 exposure and/or structural oxygen of Au/$FePO_4$. To clarify which is the case, $C^{16}O$ was fed onto fresh Au/$FePO_4$ that was pretreated at 200 °C in $^{18}O_2$ and then cooled in $^{18}O_2$ followed by purging with He at rt. This CO exposure resulted in the production of $C^{16}O_2$ but not $C^{16}O^{18}O$, suggesting the absence of either

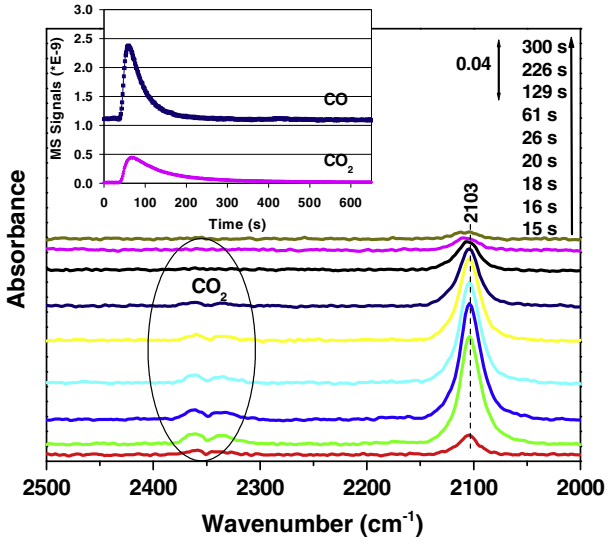

Fig. 4. IR spectra and QMS (inset) results of a pulse of CO at rt onto H_2-pretreated Au/$FePO_4$ as a function of time.

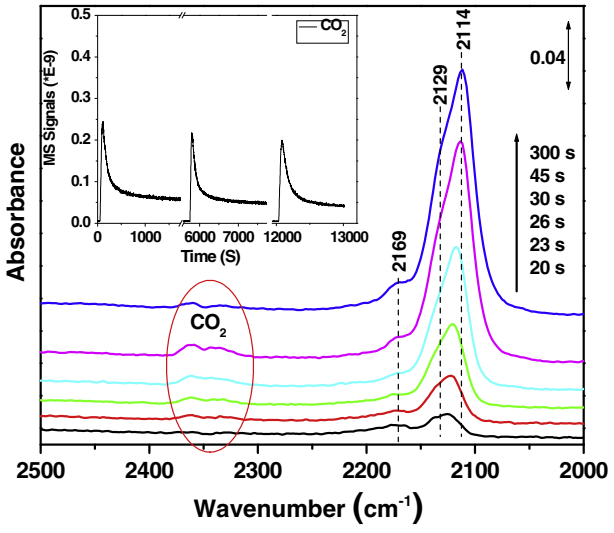

Fig. 5. IR spectra obtained during the second CO adsorption switch at rt on an O_2-pretreated Au/$FePO_4$ after an initial CO adsorption/desorption cycle. The inset shows the QMS (CO_2) response during this second adsorption and two subsequent adsorptions, each separated by an intermediate interval of rt O_2 exposure.

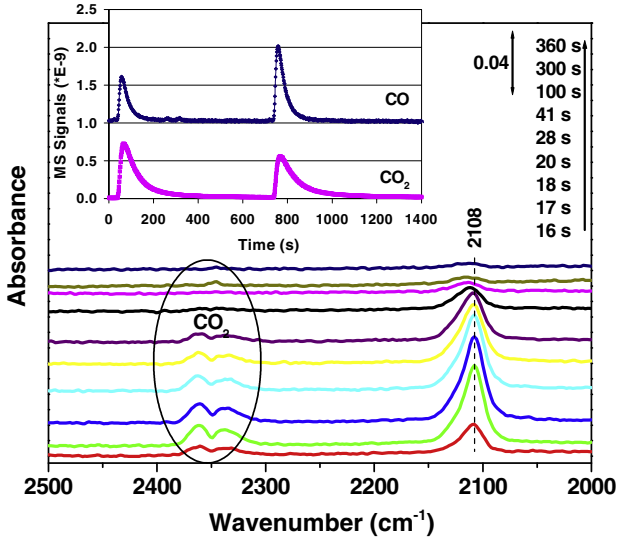

Fig. 6. IR spectra obtained during the first pulse of CO on $Au/FePO_4$ which was pretreated as follows: first H_2-pretreatment at 200 °C, then exposure to O_2 flow at rt for 30 min followed by He purging for 30 min. The inset shows the QMS (CO_2) response during the first and the subsequent CO pulses.

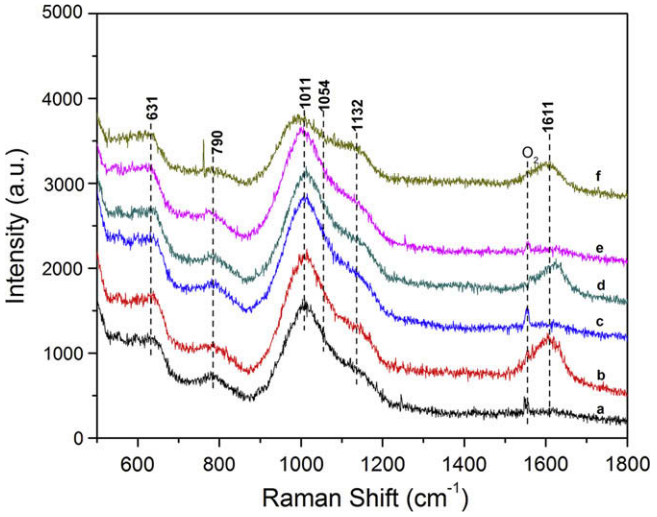

Fig. 7. Raman spectra of $Au/FePO_4$ obtained at rt after various treatments: (a) pretreated with O_2 in He; (b) after introducing 1%CO/He onto O_2-pretreated sample; (c) switching to O_2; (d) switching back to CO; (e) introducing CO and O_2 onto O_2-pretreated sample; and (f) H_2-pretreated sample in He. Gas phase O_2 is visible as a narrow peak at 1555 cm^{-1}.

chemisorption of ^{18}O and peroxides or incorporation of ^{18}O into the $Au/FePO_4$ during the pretreatment in $^{18}O_2$. Therefore, the active oxygen species responsible for the evolution of CO_2 in Fig. 5 must have originated from structural oxygen of the $FePO_4$ support in the as-synthesized sample, and furthermore, CO is able to remove it. The possibility that the active oxygen originated from an impurity Fe_2O_3 could be excluded because no Fe_2O_3 phase was observed in XRD, and the Fe:P ratio measured by ICP on the $FePO_4$ support was about one, which is consistent with the absence of non-P-containing Fe compounds. In addition, rt CO adsorption experiments were conducted over an Au/Fe_2O_3 catalyst and in that case no production of CO_2 was observed.

That structural oxygen is exchanged following rt CO exposure and CO_2 evolution was confirmed by Raman experiments shown in Fig. 7. The Raman spectrum of the O_2-pretreated $Au/FePO_4$ (Fig. 7a) exhibits peaks at 631 and 790, and an intense one at 1011 cm^{-1} with shoulders at 1054 and 1132 cm^{-1}. Generally, the stretching and bending vibrations of phosphate groups occur at 1000–1200 and 400–800 cm^{-1}, respectively. Raman bands at 1011 and 1054 cm^{-1} can be attributed to alternately connected tetrahedral PO_4 and FeO_4 groups, respectively [43,44]. The bands at 1132 and 631 cm^{-1} can be ascribed to the presence of metaphosphate, which is commonly observed in iron phosphate. When the $Au/FePO_4$ is pretreated with H_2 at 200 °C, (Fig. 7f), the obvious changes in the spectrum are the appearance of a new band at 1610 cm^{-1}, and the bands at 1011 and 1054 cm^{-1} red shift and decrease in intensity. These spectral changes are most likely due to the reduction of $FePO_4$. No Raman band is reported for iron phosphate in the range around 1600 cm^{-1}, and thus the exact assignment of the band at 1610 cm^{-1} is not clear presently. Nevertheless, the band at 1610 cm^{-1} is herein regarded as a signature for the reduction of $FePO_4$. When the O_2-treated $Au/FePO_4$ is exposed to flowing CO at rt, the band at 1610 cm^{-1} is also observed (Fig. 7b), but it disappears when the gas flow is switched to O_2 (Fig. 7c). This band is not due to the surface carbonate species that are formed from CO adsorption. If such a carbonate species were present it should be stable in oxygen and therefore should be observed in Fig. 7c. Instead, this band is an indication of the reduction of $FePO_4$. Since the major structural bands due to $FePO_4$ at 1011 and 1054 cm^{-1} do not change in position and relative intensity, it seems that the reduction by CO at rt is restricted to the surface region of $FePO_4$. Also, the addition of oxygen at rt (Fig. 7c) does not lead to any new features or change in the spectrum that could be interpreted as due to the presence of peroxides or superoxides, expected near 1128 and 883 cm^{-1}, respectively [45,46]. During repeated CO–O_2 switching cycles, the band at 1610 cm^{-1} repeats the behavior of appearing and disappearing (Fig. 7b-d), suggesting that the oxygen in $FePO_4$ can be consumed by CO and then replenished by gaseous O_2 at rt. When CO and O_2 (CO:O_2 = 1:4) are co-fed, the spectrum of $Au/FePO_4$ resembles that of the O_2-pretreated sample (Fig. 7e), implying that the rt reoxidation cycle is fast, and that the $FePO_4$ remains oxidized under these conditions.

The rt redox property of $FePO_4$ in $Au/FePO_4$ is quite surprising because $FePO_4$ usually shows redox behavior only at temperatures above 250 °C in various oxidation and oxidative dehydrogenation reactions [43,47–49]. In those cases, the charge-state of iron is critical to the reaction mechanism (*via* a Mars–van Krevelen type of reaction mechanism, possibly involving an Fe^{3+}/Fe^{2+} redox couple) and performance [47,50,51]. We conclude that the rt redox property of $FePO_4$ must be related to the presence of Au. This conclusion is supported by the contrasting behavior of both CO and O_2 adsorptions on $Au/FePO_4$ *vs* $FePO_4$. No IR bands due to adsorbed CO and no gas phase CO_2 were ever detected when flowing CO over Au-free $FePO_4$ at rt, whether it was pretreated with O_2 or H_2. Pulsed O_2 chemisorption was performed to measure O_2 uptake, and the results show that H_2-pretreated $Au/FePO_4$ catalyst adsorbed 32 μmol O_2/g catalyst at rt, while similarly pretreated Au-free $FePO_4$ did not chemisorb detectable amounts of O_2. It seems that the surface Au helps activate both CO and O_2 so that the $FePO_4$ support can undergo cycles of reduction (by CO) and reoxidation (by O_2).

3.3. CO oxidation reaction on $Au/FePO_4$

To determine the role of the redox property of $Au/FePO_4$ and the state of Au species during continuous CO oxidation reaction, $^{16}O_2$-treated $Au/FePO_4$ was used to catalyze CO oxidation by labeled $^{18}O_2$ at rt. As shown in Fig. 8 two bands at 2360 and 2340 cm^{-1}, assigned to gaseous $C^{16}O_2$, appear immediately after introducing CO and $^{18}O_2$. This unlabeled CO_2 may derive from both the reduction of cationic Au by CO and the reaction between CO and structural oxygen of $FePO_4$. As the reaction proceeds, IR bands at 2340 and

2325 cm^{-1}, due to $C^{16}O^{18}O$, grow in parallel with the band at 2114 cm^{-1} ($CO–Au^0$). The $C^{16}O^{18}O$ is produced from the Au-catalyzed reaction between CO and the incoming $^{18}O_2$. The intensity of the gas phase band at 2360 cm^{-1} ($C^{16}O_2$) maximizes at about 90 s and then decreases with time on stream due to the limited ^{16}O source on the surface. Correspondingly, the QMS signal (inset in Fig. 8) due to $C^{16}O_2$ ($m/e = 44$) increases simultaneously with the signal due to CO ($m/e = 28$) and decreases after about 90 s. The appearance of $C^{16}O^{18}O$ ($m/e = 46$) is delayed relative to $C^{16}O_2$ but dominates CO_2 production at prolonged reaction time.

The parallel growth of the IR bands due to $C^{16}O^{18}O$ (2325 cm^{-1}) and $CO–Au^0$ (2114 cm^{-1}) suggests that the production of $C^{16}O^{18}O$ takes place only after metallic Au is formed from the reduction of cationic Au by CO. This points to the positive catalytic role of metallic Au in rt CO oxidation on $Au/FePO_4$, and is confirmed by a control experiment conducted over a 200 °C H_2-pretreated sample whose surface is dominated by metallic Au. Fig. 9 shows the onset of reaction when a $CO–^{18}O_2$ mixture is switched into the H_2-pretreated sample. In this case, IR bands and QMS signals due to $C^{16}O_2$, $C^{16}O^{18}O$, and even $C^{18}O^{18}O$ are observed simultaneously from the very beginning of the reaction. This implies that CO reacts with structural oxygen of $FePO_4$ and activated $^{18}O_2$ from the onset when metallic Au exists on the surface. The simultaneous appearance of $C^{16}O_2$ and $C^{16}O^{18}O$ suggests that two reaction pathways exist: (1) a redox pathway in which $FePO_4$ supplies active O, and (2) a direct pathway in which gas phase O_2 provides the active O occurring on a metallic Au surface *via* either a Langmuir–Hinshelwood mechanism or an Eley–Rideal reaction mechanism.

It is apparent from both Figs. 8 and 9 that a substantial amount of $C^{18}O^{18}O$ is formed under these reaction conditions, which is relatively more on the H_2-pretreated sample than on the O_2-pretreated sample. This product cannot be formed directly from the reaction of $C^{16}O$ and $^{18}O_2$ (direct pathway) or by the reaction of $C^{16}O$ with the ^{16}O-loaded phosphate support (redox pathway), and therefore a mechanism for isotope scrambling must exist. There are two additional indications of isotope scrambling. First, the QMS indicates the presence of $C^{18}O$ in the product stream. On the H_2-pretreated catalyst, this component builds up almost simultaneously with the CO_2 products on the surface (Fig. 9), whereas on the O_2-pretreated surface it lags behind the growth of the direct product ($CO^{18}O$) and the redox product (CO_2) but precedes the $C^{18}O^{18}O$ product (Fig. 8). Second, the FTIR spectrum shown in Fig. 8 exhibits a peak at 2065 cm^{-1} that grows with exposure time and may be attributed to $C^{18}O$ adsorption. The likely source of isotope scrambling is the adsorption of product dioxide on the support to form a carbonate-like species on the surface followed by oxygen exchange and subsequent decomposition. Such ephemeral growth of carbonate from gas phase CO_2 has been reported on oxide-supported catalysts, for example, in Au/TiO_2 [52–54] and Au/Al_2O_3 catalysts [53]. Because the yield of the scrambled products is relatively larger for the H_2-pretreated catalyst, the scrambling must be more facile on this surface than on the O_2-pretreated catalyst. This is attributed to the H_2-induced reduction of the phosphate support, which is expected to make it more susceptible to carbonate formation. The delayed production of the mixed dioxide products on the O_2-pretreated surface can now be understood to be related to two factors. First, the initial dearth of catalytically active metallic Au causes a delay of the $CO^{18}O$ relative to the CO_2, but this delay also lengthens the time required to displace ^{16}O from the phosphate and replace it with ^{18}O by carbonate exchange, which is necessary to create the $C^{18}O^{18}O$ product.

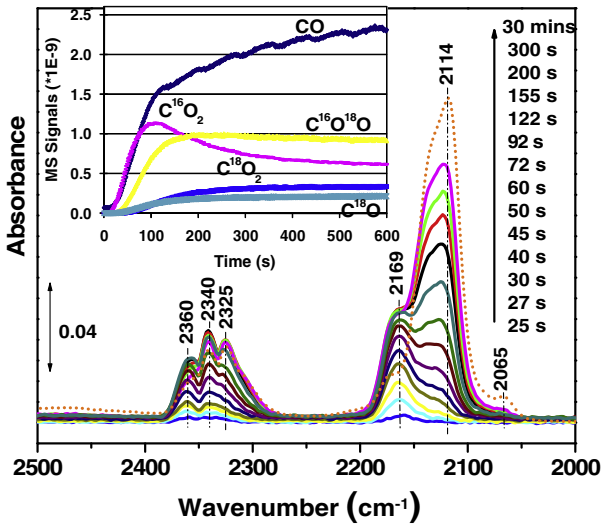

Fig. 8. IR spectra and QMS (inset) results following switch from He to CO + $^{18}O_2$ at rt as a function of time after the switch. The $Au/FePO_4$ catalyst was pretreated in $^{16}O_2$ at 200 °C.

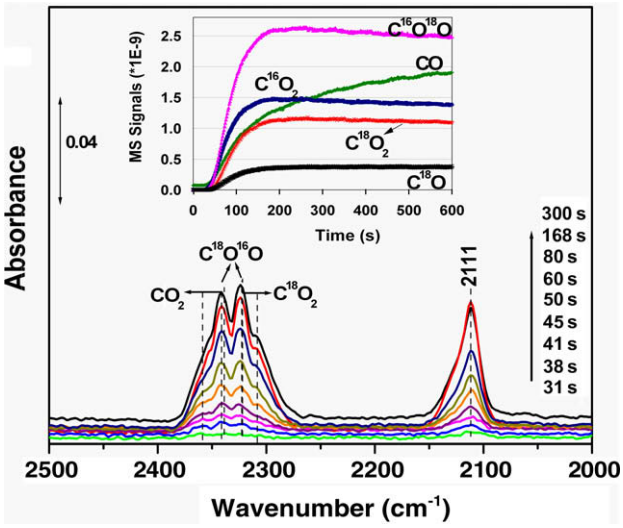

Fig. 9. IR spectra and QMS (inset) results following switch from He to CO + $^{18}O_2$ at rt as a function of time after the switch. The $Au/FePO_4$ catalyst was pretreated in H_2 at 200 °C.

4. Discussion

4.1. Nature of surface Au sites

The present results show that different treatments of $Au/FePO_4$ lead to as many as four different CO adsorption frequencies, each signaling a different Au adsorption environment. Cationic Au is present after oxidative treatment, and metallic Au dominates after reductive treatment. Evidence for cationic Au on the O_2-pretreated sample is derived from both XANES and the high-frequency CO adsorption peak (2169 cm^{-1}) observed upon initial CO adsorption [55,56]. The majority of this cationic Au undergoes *in situ* reduction to metallic Au during rt CO adsorption, leaving CO adsorption peaks at 2129 and 2114 cm^{-1}. The cationic Au is hypothesized to be isolated or clustered Au oxide particles remaining from the DP process and subsequent O_2-pretreatment at 200 °C that removes hydroxyls. A peak at 2129 cm^{-1} may be associated with positively polarized Au affected by nearby oxygen, whereas the peak at

2114 cm^{-1} is attributable to metallic Au [55]. These two peaks were always found together, i.e. a single isolated peak at 2114 cm^{-1} was never observed. H_2-pretreatment at 200 °C also leads to a metallic Au state characterized by a single CO peak position of 2103 cm^{-1}. The two different types of metallic Au on the differently prepared samples, as probed by CO stretching frequency, may be related to the presence or absence of coexisting positively polarized Au. Reduction to metallic Au is essentially irreversible since following H_2-pretreatment even extended high temperature treatments in O_2 do not recover oxidized Au.

It is apparent that for the sample containing only reduced Au, i.e. the H_2-pretreated Au/$FePO_4$, the CO frequency is unaltered by the amount (coverage) of adsorbed CO as demonstrated in Fig. 4. Such insensitivity would seem to indicate that the adsorbed CO molecules must be isolated from dipolar interactions with neighboring CO. One possible explanation for the insensitivity is that the CO molecules may be oriented in a variety of spatial orientations thereby minimizing dipolar interactions. Coverage dependence in CO stretching frequency was reported on single-crystal Au surfaces where CO molecules are expected to be spatially aligned [57,58], but others reported little or no coverage dependence [59]. Meier and Goodman [60] reported that the vibrational frequency for CO adsorbed on Au clusters grown on model flat TiO_2 surfaces was nearly invariant with CO coverage and Au cluster size even though the CO adsorption energy is both coverage-dependent and cluster size-dependent. However, in dispersed Au/TiO_2 the CO frequency is observed to vary with coverage [52]. Evidently the coverage dependence is affected by factors that may still not be well understood.

Although the reduced Au obtained on the H_2-pretreated sample exhibits a coverage-independent peak at 2103 cm^{-1} during CO adsorption, this position is altered by oxygen. After exposure of the H_2-pretreated sample to O_2 at rt, the CO stretching frequency observed during the first CO pulse is blue-shifted to 2108 cm^{-1}, a position that is again independent of CO coverage (Fig. 6). Subsequent pulses of CO cause a gradual shift of the CO frequency back to 2103 cm^{-1}. If instead, the H_2-pretreated sample is first exposed to an O_2-rich reaction mixture, the CO frequency in this case is also blue-shifted (relative to CO adsorption) and appears at 2111 cm^{-1} (Fig. 9). These shifts of about 5–8 cm^{-1}, resulting from either pre-adsorbed or co-fed O_2, are attributed to the effect of oxidation of the phosphate support. The reversible shifts between 2108 and 2103 cm^{-1} during pulsed CO adsorption are attributed to the dynamic variation in the phosphate, adjacent to the Au, as it undergoes structural oxygen transfer by CO reduction. In particular, the shift is not attributed to any change in the oxidation state of the Au since the shift is quite small and the frequencies are in the right range for adsorbed CO on metallic Au [41]. Neither is it attributed to the presence of O_2-like species adsorbed on the Au as is discussed below. Apparently, the frequency of adsorbed CO on Au depends not only on the oxidation state of surface Au sites but also on the reduction degree of the support, a new phenomenon not remarked upon for other supported Au catalysts.

4.2. CO oxidation mechanism

The above information on the nature of surface Au sites on $FePO_4$ is critical for revealing the reaction mechanism of CO oxidation, including the catalytically active Au sites and the reaction pathways. The IR-QMS measurement during rt CO oxidation with labeled $^{18}O_2$ on these differently treated samples shows that metallic Au catalyzes the direct reaction of CO with O_2, while both cationic and metallic Au catalyze the redox reaction of CO with structural O of $FePO_4$. Previously reported spectroscopic data have provided evidence of various types of Au sites on oxide supports for CO adsorption, including zero-valent, anionic, and cationic gold, present together [10,61] or as a single type [62–65]. It has been proposed that CO oxidation activity increases consistently as the CO band shifts to lower wavenumbers for an Au/SiO_2 catalyst [6], implying that the activity correlates with the reduction degree of surface Au. This kind of correlation was also observed for CO oxidation on Au/TiO_2 [8]. However, there is also strong evidence for the involvement of cationic gold in Au catalysis [16]. On the present Au/$FePO_4$ catalyst, there is no indication of a positive role of cationic Au in CO oxidation *via* the direct mechanism.

Early work on catalysis by Au suggested that the use of reducible oxide supports could lead to more active catalysts [66]. Although the differences in activities for reducible supports have been noted and their role in activating oxygen has been suggested [21,22], there is little clear evidence that a Mars–van Krevelen (redox) reaction mechanism plays a role in the low temperature CO oxidation reactions catalyzed by Au. Participation of support oxygen in the low temperature CO oxidation is rarely reported even when Au is supported on the so-called "active" *oxide* supports. Support-induced activation of oxygen has been reported to occur on Fe doped TiO_2 [45] and nanocrystalline CeO_2 [67], and in these cases the presence of Au enhances the activation of oxygen through the formation of adsorbed peroxide and superoxide at the metal–oxide interface. In the present experiments we found no evidence that the active oxygen is due to adsorbed oxygen in any form. Pre-adsorption of $^{18}O_2$at rt did not give rise to mixed $C^{18}O^{16}O$ formation during subsequent CO exposure, and Raman failed to find evidence of peroxide or superoxide after O_2 exposure. Instead, we found evidence of Au-catalyzed oxidation of CO by active, structural oxygen from the phosphate support.

5. Conclusions

The nature of Au species on an Au/$FePO_4$ catalyst after oxidative and reductive pretreatments as well as their role in rt CO oxidation has been investigated using gas transient and *operando* DRIFTS-QMS and *in situ* Raman spectroscopy. Oxidative pretreatment (in O_2) leads to cationic Au species that can be reduced by CO at rt. *In situ* reduction of the cationic Au during CO oxidation generates metallic Au that is active for CO oxidation. Reductive pretreatment (in H_2) leads to metallic Au species that are more active for CO oxidation than those on an oxidatively pretreated catalyst. CO oxidation results demonstrate that CO can be oxidized by structural O of $FePO_4$ and that O_2 can be activated by the thusly reduced support. Au assists in and is essential for both the utilization of structural oxygen and the activation of O_2. Isotope studies using $^{18}O_2$ demonstrate that the redox pathway occurs in competition with the direct reaction catalyzed by metallic Au. To our knowledge, this is the first clear evidence of a redox pathway playing a role in CO oxidation by Au catalysts.

Acknowledgments

This work was sponsored by the Division of Chemical Sciences, Geosciences, and Biosciences, Office of Basic Energy Sciences, US Department of Energy, under Contract DE-AC05-00OR22725 with Oak Ridge National Laboratory, managed and operated by UT-Battelle, LLC. A portion of this research was done using facilities at the Center for Nanophase Materials Sciences. XANES measurements were performed at the National Synchrotron Light Source, Brookhaven National Laboratory supported by the US Department of Energy, Office of Science, Office of Basic Energy Sciences, under Contract No. DE-AC02-98CH10886, and using facilities of the Synchrotron Catalysis Consortium, supported by US Department of Energy Grant No. DE-FG02-05ER15688.

References

[1] M. Haruta, T. Kobayashi, H. Sano, N. Yamada, Chemistry Letters (1987) 405.
[2] G.C. Bond, D.T. Thompson, Catalysis Reviews – Science and Engineering 41 (1999) 319.
[3] G.C. Bond, C. Louis, D.T. Thompson, Catalysis by Gold, Imperial College Press, London, 2006.
[4] M.C. Kung, R.J. Davis, H.H. Kung, Journal of Physical Chemistry C 111 (2007) 11767.
[5] V. Schwartz, D.R. Mullins, W.F. Yan, B. Chen, S. Dai, S.H. Overbury, Journal of Physical Chemistry B 108 (2004) 15782.
[6] Z. Wu, S. Zhou, H. Zhu, S. Dai, S.H. Overbury, Chemical Communications 2008 (2008) 3308.
[7] F. Boccuzzi, A. Chiorino, S. Tsubota, M. Haruta, Journal of Physical Chemistry 100 (1996) 3625.
[8] J.H. Yang, J.D. Henao, M.C. Raphulu, Y.M. Wang, T. Caputo, A.J. Groszek, M.C. Kung, M.S. Scurrell, J.T. Miller, H.H. Kung, Journal of Physical Chemistry B 109 (2005) 10319.
[9] N. Weiher, A.M. Beesley, N. Tsapatsaris, L. Delannoy, C. Louis, J.A. van Bokhoven, S.L.M. Schroeder, Journal of the American Chemical Society 129 (2007) 2240.
[10] J. Guzman, B.C. Gates, Journal of the American Chemical Society 126 (2004) 2672.
[11] Q. Fu, H. Saltsburg, M. Flytzani-Stephanopoulos, Science 301 (2003) 935.
[12] J. Guzman, B.C. Gates, Journal of Physical Chemistry B 106 (2002) 7659.
[13] G.J. Hutchings, M.S. Hall, A.F. Carley, P. Landon, B.E. Solsona, C.J. Kiely, A. Herzing, M. Makkee, J.A. Moulijn, A. Overweg, J.C. Fierro-Gonzalez, J. Guzman, B.C. Gates, Journal of Catalysis 242 (2006) 71.
[14] C.K. Costello, M.C. Kung, H.-S. Oh, Y. Wang, H.H. Kung, Applied Catalysis A – General 232 (2002) 159.
[15] A.M. Venezia, G. Pantaleo, A. Longo, G. Di Carlo, M.P. Casaletto, F.L. Liotta, G. Deganello, Journal of Physical Chemistry B 109 (2005) 2821.
[16] J.C. Fierro-Gonzalez, B.C. Gates, Catalysis Today 122 (2007) 201.
[17] A.A. Herzing, C.J. Kiely, A.F. Carley, P. Landon, G.J. Hutchings, Science 321 (2008) 1331.
[18] M.S. Chen, D.W. Goodman, Science 306 (2004) 252.
[19] S.H. Overbury, V. Schwartz, D.R. Mullins, W.F. Yan, S. Dai, Journal of Catalysis 241 (2006) 56.
[20] S.N. Rashkeev, A.R. Lupini, S.H. Overbury, S.J. Pennycook, S.T. Pantelides, Physical Review B 76 (2007) 035438.
[21] S.H. Overbury, L. Ortiz-Soto, H.G. Zhu, B. Lee, M.D. Amiridis, S. Dai, Catalysis Letters 95 (2004) 99.
[22] M.M. Schubert, S. Hackenberg, A.C. van Veen, M. Muhler, V. Plzak, R.J. Behm, Journal of Catalysis 197 (2001) 113.
[23] H.G. Zhu, C.D. Liang, W.F. Yan, S.H. Overbury, S. Dai, Journal of Physical Chemistry B 110 (2006) 10842.
[24] M. Okumura, S. Nakamura, S. Tsubota, T. Nakamura, M. Azuma, M. Haruta, Catalysis Letters 51 (1998) 53.
[25] I.N. Remediakis, N. Lopez, J.K. Nørskov, Applied Catalysis A – General 291 (2005) 13.
[26] N. Lopez, J.K. Nørskov, Surface Science 515 (2002) 175.
[27] H.L. Lian, M.J. Jia, W.C. Pan, Y. Li, W.X. Zhang, D.Z. Jiang, Catalysis Communications 6 (2005) 47.
[28] N. Phonthammachai, Z. Ziyi, G. Jun, H.Y. Fan, T.J. White, Gold Bulletin 41 (2008) 42.
[29] A. Venugopal, M.S. Scurrell, Applied Catalysis A – General 245 (2003) 137.
[30] Y.-F. Han, N. Phonthammachai, K. Ramesh, Z. Zhong, T. White, Environmental Science and Technology 42 (2008) 908.
[31] J. Liu, W. Chen, X. Liu, K. Zhou, Y. Li, Nano Research 1 (2008) 46.
[32] H.G. Zhu, Z. Ma, J.C. Clark, Z.W. Pan, S.H. Overbury, S. Dai, Applied Catalysis A – General 326 (2007) 89.
[33] G. Budroni, A. Corma, Angewandte Chemie – International Edition 45 (2006) 3328.
[34] W.F. Yan, S. Brown, Z.W. Pan, S.M. Mahurin, S.H. Overbury, S. Dai, Angewandte Chemie – International Edition 45 (2006) 3614.
[35] Z. Ma, H. Yin, S.H. Overbury, S. Dai, Catalysis Letters 126 (2008) 20.
[36] M. Ai, Catalysis Today 85 (2003) 193.
[37] F.M. Bautista, J.M. Campelo, A. Garcia, D. Luna, J.M. Marinas, R.A. Quiros, A.A. Romero, Applied Catalysis A – General 243 (2003) 93.
[38] F.M. Bautista, J.M. Campelo, D. Luna, J.M. Marinas, R.A. Quiros, A.A. Romero, Applied Catalysis B – Environmental 70 (2007) 611.
[39] F. Boccuzzi, A. Chiorino, M. Manzoli, D. Andreeva, T. Tabakova, Journal of Catalysis 188 (1999) 176.
[40] S. Minico, S. Scire, C. Crisafulli, A.M. Visco, S. Galvagno, Catalysis Letters 47 (1997) 273.
[41] K.I. Hadjiivanov, G.N. Vayssilov, Characterization of oxide surfaces and zeolites by carbon monoxide as an IR probe molecule, Advances in Catalysis, vol. 47, Academic Press Inc., San Diego, 2002, p. 307.
[42] M. Englisch, J.A. Lercher, G.L. Haller, in: Y. Iwasawa (Ed.), X-ray Absorption Fine Structure for Catalysts and Surfaces, World Scientific Publishing, New Jersey, 1996, p. 276.
[43] P. Nagaraju, N. Lingaiah, A. Balaraju, P.S.S. Prasad, Applied Catalysis A – General 339 (2008) 99.
[44] D.H. Yu, C. Wu, Y. Kong, N.H. Xue, X.F. Guo, W.P. Ding, Journal of Physical Chemistry C 111 (2007) 14394.
[45] S. Carrettin, Y. Hao, V. Aguilar-Guerrero, B.C. Gates, S. Trasobares, J.J. Calvino, A. Corma, Chemistry – A European Journal 13 (2007) 7771.
[46] V.V. Pushkarev, V.I. Kovalchuk, J.L. d'Itri, Journal of Physical Chemistry B 108 (2004) 5341.
[47] A.M. Beale, G. Sankar, Journal of Materials Chemistry 12 (2002) 3064.
[48] J.M.M. Millet, J.C. Vedrine, Topics in Catalysis 15 (2001) 139.
[49] E. Muneyama, A. Kunishige, K. Ohdan, M. Ai, Journal of Catalysis 158 (1996) 378.
[50] M. Dekiouk, N. Boisdron, S. Pietrzyk, Y. Barbaux, J. Grimblot, Applied Catalysis A – General 90 (1992) 61.
[51] C. Virely, M. Forissier, J.M.M. Millet, J.C. Vedrine, D. Huchette, Journal of Molecular Catalysis 71 (1992) 199.
[52] J.C. Clark, S. Dai, S.H. Overbury, Catalysis Today 126 (2007) 135.
[53] J.T. Calla, M.T. Bore, A.K. Datye, R.J. Davis, Journal of Catalysis 238 (2006) 458.
[54] J.D. Henao, T. Caputo, J.H. Yang, M.C. Kung, H.H. Kung, Journal of Physical Chemistry B 110 (2006) 8689.
[55] M. Mihaylov, B.C. Gates, J.C. Fierro-Gonzalez, K. Hadjiivanov, H. Knozinger, Journal of Physical Chemistry C 111 (2007) 2548.
[56] T. Venkov, H. Klimev, M.A. Centeno, J.A. Odriozola, K. Hadjiivano, Catalysis Communications 7 (2006) 308.
[57] D.C. Meier, V. Bukhtiyarov, A.W. Goodman, Journal of Physical Chemistry B 107 (2003) 12668.
[58] C. Ruggiero, P. Hollins, Journal of the Chemical Society – Faraday Transactions 92 (1996) 4829.
[59] Y. Jugnet, F. Aires, C. Deranlot, L. Piccolo, J.C. Bertolini, Surface Science 521 (2002) L639.
[60] D.C. Meier, D.W. Goodman, Journal of the American Chemical Society 126 (2004) 1892.
[61] F. Vindigni, M. Manzoli, A. Chiorino, T. Tabakova, F. Boccuzzi, Journal of Physical Chemistry B 110 (2006) 23329.
[62] C.K. Costello, J. Guzman, J.H. Yang, Y.M. Wang, M.C. Kung, B.C. Gates, H.H. Kung, Journal of Physical Chemistry B 108 (2004) 12529.
[63] D.A.H. Cunningham, W. Vogel, H. Kageyama, S. Tsubota, M. Haruta, Journal of Catalysis 177 (1998) 1.
[64] M. Mihaylov, E. Ivanova, Y. Hao, K. Hadjiivanov, B.C. Gates, H. Knozinger, Chemical Communications (2008) 175.
[65] B. Yoon, H. Hakkinen, U. Landman, A.S. Worz, J.M. Antonietti, S. Abbet, K. Judai, U. Heiz, Science 307 (2005) 403.
[66] M. Haruta, S. Tsubota, T. Kobayashi, H. Kageyama, M.J. Genet, B. Delmon, Journal of Catalysis 144 (1993) 175.
[67] J. Guzman, S. Carrettin, J.C. Fierro-Gonzalez, Y.L. Hao, B.C. Gates, A. Corma, Angewandte Chemie – International Edition 44 (2005) 4778.